



Evaluating the timing and structure of the 4.2 ka event in the Indian summer monsoon domain from an annually resolved speleothem record from Northeast India

Gayatri Kathayat¹, Hai Cheng^{1,2}, Ashish Sinha³, Max Berkelhammer⁴, Haiwei Zhang¹, Pengzhen Duan¹, Hanying Li¹, Xianglei Li¹, Youfeng Ning¹, and R. Lawrence Edwards²

¹Institute of Global Environmental Change, Xi'an Jiaotong University, Xi'an, China

²Department of Earth Sciences, University of Minnesota, Minneapolis, USA

³Department of Earth Science, California State University Dominguez Hills, Carson, USA

⁴Department of Earth and Environmental Sciences, University of Illinois, Chicago, USA

Correspondence: Gayatri Kathayat (kathayat@xjtu.edu.cn) and Hai Cheng (cheng021@xjtu.edu.cn)

Received: 23 July 2018 – Discussion started: 16 August 2018

Revised: 12 November 2018 – Accepted: 17 November 2018 – Published: 30 November 2018

Abstract. A large array of proxy records suggests that the “4.2 ka event” marks an approximately 300-year long period (~ 3.9 to 4.2 ka) of major climate change across the globe. However, the climatic manifestation of this event, including its onset, duration, and termination, remains less clear in the Indian summer monsoon (ISM) domain. Here, we present new oxygen isotope ($\delta^{18}\text{O}$) data from a pair of speleothems (ML.1 and ML.2) from Mawmluh Cave, Meghalaya, India, that provide a high-resolution record of ISM variability during a period (~ 3.78 and 4.44 ka) that fully encompasses the 4.2 ka event. The sub-annually to annually resolved ML.1 $\delta^{18}\text{O}$ record is constrained by 18 ^{230}Th dates with an average dating error of ± 13 years (2σ) and a resolution of ~ 40 years, which allows us to characterize the ISM variability with unprecedented detail. The inferred pattern of ISM variability during the period contemporaneous with the 4.2 ka event shares broad similarities and key differences with the previous reconstructions of ISM from the Mawmluh Cave and other proxy records from the region. Our data suggest that the ISM intensity, in the context of the length of our record, abruptly decreased at ~ 4.0 ka ($\sim \pm 13$ years), marking the onset of a multi-centennial period of relatively reduced ISM, which was punctuated by at least two multi-decadal droughts between ~ 3.9 and 4.0 ka. The latter stands out in contrast with some previous proxy reconstructions of the ISM, in which the 4.2 ka event has been depicted as a singular multi-centennial drought.

1 Introduction

The time interval between 4.2 and 3.9 ka (thousand of years before present, where present is 1950 CE) constitutes an important period from both climatological and archeological perspectives (e.g., Weiss et al., 1993; Cullen et al., 2000; Staubwasser et al., 2003; Berkelhammer et al., 2012; Weiss, 2016). A global suite of proxy records shows widespread climate anomalies during the time (commonly referred to as the “4.2 ka event”; e.g., Cullen et al., 2000; Staubwasser et al., 2003; Arz et al., 2006; Drysdale et al., 2006; Menounos et al., 2008; Liu and Feng, 2012; Berkelhammer et al., 2012; Dixit et al., 2014, 2018; Cheng et al., 2015; Nakamura et al., 2016; Railsback et al., 2018). Additionally, a number of archeological studies also suggest that the 4.2 ka event was associated with a series of cultural and societal changes in the Mediterranean, Middle East, Africa, and South and East Asia (e.g., Weiss et al., 1993; Enzel et al., 1999; Cullen et al., 2000; Staubwasser et al., 2003; Marshall et al., 2011; Liu and Feng, 2012; Dixit et al., 2014; Weiss, 2016). For example, the 4.2 ka event has been proposed to have contributed to collapses of the early Bronze Age civilizations, including the Longshan culture in China (Chang, 1999; Liu and Feng, 2012), the Egyptian Old Kingdom by the Nile River (Stanley et al., 2003), and the Akkadian Empire in Mesopotamia (Weiss et al., 1993; Cullen et al., 2000). In South Asia, the 4.2 ka event has been linked to a weakening of the Indian summer monsoon (ISM) and the ensuing de-urbanization

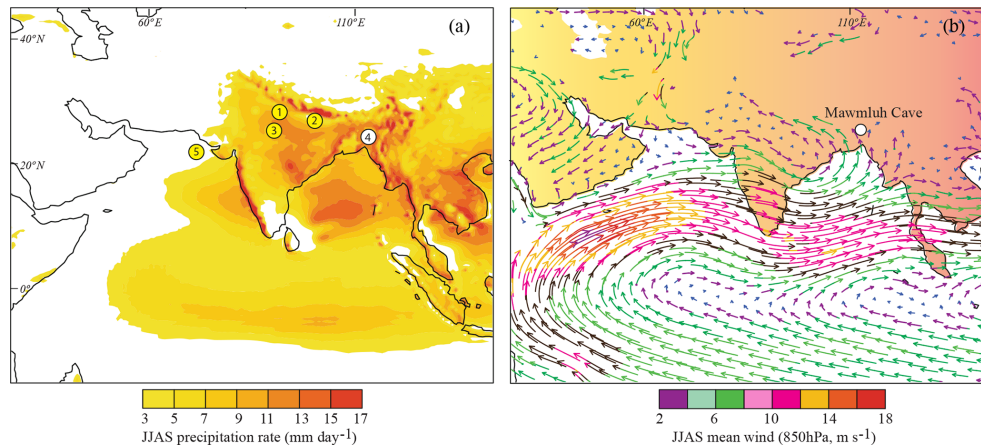


Figure 1. Location map and spatial structure of mean JJAS precipitation and low-level winds. **(a)** June–July–August–September (JJAS) precipitation from the Tropical Rainfall Measuring Mission (TRMM). The locations of Mawmluh Cave (white circle) and other proxy records mentioned in the text (yellow circles and numbers). The numbering scheme is as follows: 1, Sahiya Cave (Kathayat et al., 2017); 2, Lake Rara (Nakamura et al., 2016); 3, Kotla Dhar (Dixit et al., 2014); 4, Mawmluh Cave (Berkelhammer et al., 2012); and 5, Indus Delta (Staubwasser et al., 2003). **(b)** The 850 hPa monsoon vector from zoomed Laboratoire de Meteorologie Dynamique (LMDZ) general circulation model with telescoping zooming (figure adapted and modified from Sabin et al., 2013). The zoom version shows a well-defined cyclonic circulation with westerlies on the southern flanks and easterly winds on the northern flanks of the monsoon trough. The Mawmluh Cave is ideally located to record upstream variations in the overall strength of the ISM (see text).

of the Indus Valley Civilization (Staubwasser et al., 2003; Madella and Fuller, 2006; Dixit et al., 2014, 2018; Giosan et al., 2012; Berkelhammer et al., 2012; Kathayat et al., 2017).

A number of proxy records from the Indian subcontinent suggest that a major weakening of the ISM occurred around the 4.2 ka event (Staubwasser et al., 2003; Berkelhammer et al., 2012; Dixit et al., 2014; Nakamura et al., 2016; Kathayat et al., 2017; Figs. 1 and 2). The 4.2 ka event has been generally described as an approximately 2- to 3-centuries-long interval of drought (e.g., Berkelhammer et al., 2012; Dixit et al., 2014; Nakamura et al., 2016), which was superimposed on a longer-term insolation-induced weakening of the ISM during the Holocene (e.g., Kathayat et al., 2017). The timing, structure, and magnitude of the 4.2 ka event in the ISM regime, however, remain unclear because most proxy records from the region have low temporal precision and insufficient resolution to precisely characterize the event (e.g., Staubwasser and Weiss, 2006; Prasad and Enzel, 2006; Nakamura et al., 2016; Dixit et al., 2018). In addition, the 4.2 ka event is notably absent in a recent high-resolution speleothem oxygen isotope ($\delta^{18}\text{O}$) record from Sahiya Cave in northern India (Kathayat et al., 2017) that exhibits a long-term drying trend from ~ 4.2 to 3.5 ka.

A high-resolution (~ 6 years) $\delta^{18}\text{O}$ record (KM-A) from Mawmluh Cave, located in the state of Meghalaya in Northeast India, has previously provided evidence of the 4.2 ka event from the ISM domain (Berkelhammer et al., 2012). The KM-A record was recently used to formally ratify the post-4.2 ka time as the Meghalayan Age (Walker et al., 2018). However, the timing and duration of the 4.2 ka event in the KM-A record is constrained by only three ^{230}Th dates

(5048 ± 32 , 4112 ± 30 , and 3654 ± 20 ka) and, additionally, the youngest date defining the termination of the event and/or the $\delta^{18}\text{O}$ values from the top ~ 30 mm of the KM-A sample that help define the event may have been potentially affected by diagenetic changes. In this study, we present new high-resolution $\delta^{18}\text{O}$ data from two stalagmites (ML.1 and ML.2) from the same cave (Figs. 1 and 3, Table 1). The ML.1 and ML.2 $\delta^{18}\text{O}$ records span from 4.44 to 3.78 ka and 4.53 to 3.70 ka, respectively, encompassing the 4.2 ka event completely. Our new records are sub-annually to annually (ML.1) and sub-decadally resolved (ML.2) and have unprecedented chronologic constraints, which allow us to characterize the nature of ISM variability during the 4.2 ka event more precisely than previously possible.

2 Samples and methods

2.1 Cave location and climatology

Mawmluh Cave ($25^{\circ}15'32''\text{N}$, $91^{\circ}42'45''\text{E}$; 1290 m a.s.l.) is located near the town of Sohra (Cherrapunji) at the southern fringe of the Meghalayan Plateau in Northeast India (Fig. 1). The mean annual rainfall is $\sim 11\,000$ mm in the region, 70 % of which falls during the peak ISM months (June–September; Murata et al., 2007). The rainfall at the cave site during the ISM period is mainly produced by convective systems and low-level air parcels originating from the Bay of Bengal, which propagate further northward and penetrate farther into the Tibetan Plateau (Sengupta and Sarkar, 2006; Breitenbach et al., 2010). The non-monsoonal component of rainfall is trivial and consists of westerly-related moisture and recycled

Table 1. ^{230}Th dating results with the 2σ analytical error.

ML.1							
Sample number	^{238}U (ppb)	^{232}Th (ppt)	$d^{234}\text{U}^{\text{a}}$ (measured)	$^{230}\text{Th}/^{238}\text{U}$ (activity)	^{230}Th age (yr) (corrected)	$d^{234}\text{U}_{\text{initial}}^{\text{b}}$ (corrected)	^{230}Th age (yr BP) $^{\text{c}}$ (corrected)
ML.1.1F	6106 ± 6	164 ± 7	-274.2 ± 0.9	0.0251 ± 0.0001	3841 ± 14	-277 ± 1	3779 ± 14
ML.1.2F	6222 ± 6	123 ± 5	-272.3 ± 0.9	0.0256 ± 0.0001	3917 ± 13	-275 ± 1	3855 ± 13
ML.1.3F	6981 ± 9	72 ± 4	-271.8 ± 1.0	0.0257 ± 0.0001	3923 ± 12	-275 ± 1	3861 ± 12
ML.1.4F	6378 ± 7	170 ± 6	-270.3 ± 0.9	0.0258 ± 0.0001	3938 ± 14	-273 ± 1	3876 ± 14
ML.1.5F	6674 ± 8	111 ± 4	-271.5 ± 0.9	0.0259 ± 0.0001	3948 ± 11	-275 ± 1	3886 ± 11
ML.1.6F	7702 ± 10	189 ± 5	-270.1 ± 1.0	0.0260 ± 0.0001	3964 ± 11	-273 ± 1	3902 ± 11
ML.1.7F	6455 ± 7	90 ± 6	-270.7 ± 0.9	0.0260 ± 0.0001	3968 ± 14	-274 ± 1	3906 ± 14
ML.1.8F	6144 ± 7	153 ± 5	-270.3 ± 1.0	0.0261 ± 0.0001	3978 ± 13	-273 ± 1	3916 ± 13
ML.1.9F	6363 ± 7	122 ± 6	-270.0 ± 1.0	0.0262 ± 0.0001	3989 ± 15	-273 ± 1	3927 ± 15
ML.1.10F	6825 ± 9	778 ± 16	-271.5 ± 1.0	0.0264 ± 0.0001	4031 ± 12	-275 ± 1	3969 ± 12
ML.1-9a	6395 ± 6	154 ± 5	-268.7 ± 0.9	0.0267 ± 0.0001	4069 ± 13	-272 ± 1	4007 ± 13
ML.1-10a	7574 ± 8	132 ± 4	-267.8 ± 0.9	0.0272 ± 0.0001	4138 ± 12	-271 ± 1	4076 ± 12
ML.1-11a	6744 ± 6	52 ± 3	-266.2 ± 0.8	0.0279 ± 0.0001	4240 ± 11	-269 ± 1	4178 ± 11
ML.1-12a	7716 ± 8	73 ± 3	-265.1 ± 0.9	0.0286 ± 0.0001	4336 ± 11	-268 ± 1	4274 ± 11
ML.1-13a	7881 ± 9	127 ± 4	-262.9 ± 1.1	0.0290 ± 0.0001	4386 ± 13	-266 ± 1	4324 ± 13
ML.1-14a	6452 ± 9	77 ± 2	-263.8 ± 1.1	0.0294 ± 0.0001	4451 ± 14	-267 ± 1	4389 ± 14
ML.1-15a	7392 ± 10	108 ± 3	-263.4 ± 1.0	0.0294 ± 0.0001	4456 ± 11	-267 ± 1	4394 ± 11
ML.1-16a	6970 ± 9	441 ± 9	-263.5 ± 1.0	0.0297 ± 0.0001	4499 ± 12	-267 ± 1	4437 ± 12
ML.2							
ML.2-7	6633 ± 9	52 ± 3	-277.0 ± 1.1	0.0231 ± 0.0001	3541 ± 16	-280 ± 1	3479 ± 16
ML.2-8	6173 ± 7	78 ± 3	-272.6 ± 1.0	0.0254 ± 0.0001	3891 ± 13	-276 ± 1	3829 ± 13
ML.2-9	7121 ± 8	134 ± 4	-266.0 ± 1.0	0.0282 ± 0.0001	4276 ± 13	-269 ± 1	4214 ± 13
ML.2-10	6085 ± 6	2953 ± 59	-262.1 ± 1.0	0.0299 ± 0.0001	4500 ± 21	-265 ± 1	4438 ± 21
ML.2-9a	6278 ± 6	106 ± 4	-257.5 ± 1.0	0.0306 ± 0.0001	4603 ± 17	-261 ± 1	4541 ± 17

^a $\delta^{234}\text{U} = ([^{234}\text{U}/^{238}\text{U}]_{\text{activity}} - 1) \times 1000$. ^b $\delta^{234}\text{U}_{\text{initial}}$ was calculated based on ^{230}Th age (T), i.e., $\delta^{234}\text{U}_{\text{initial}} = \delta^{234}\text{U}_{\text{measured}} \times e^{1234 \times T}$. Corrected ^{230}Th ages assume the initial $^{230}\text{Th}/^{232}\text{Th}$ atomic ratio of $4.4 \pm 2.2 \times 10^{-6}$. Those are the values for a material at secular equilibrium, with the bulk earth $^{232}\text{Th}/^{238}\text{U}$ value of 3.8. The errors are arbitrarily assumed to be 50%. ^c BP stands for “before present” where the “present” is defined as the year 1950 CE.

local moisture (Breitenbach et al., 2010, 2015; Berkelhammer et al., 2012). The cave is overlain by 30–100 m thick and heavily karstified host rock (limestone, sandstone, and a 40–100 cm thick coal layer; Breitenbach et al., 2010). The soil layer above the cave is rather thin (5–15 cm) and covered mainly by grasses and bushes. Cave monitoring data (Breitenbach et al., 2010) indicate that the relative humidity inside the cave is more than 95 % even during the dry season (November to April). Temperature variations in the cave are small (18.0–18.5 °C) and close to the mean annual temperature of the area (Breitenbach et al., 2010, 2015). A 3-year cave monitoring result suggests that cave drip-water $\delta^{18}\text{O}$ signals lag corresponding local rainfall by less than 1 month and thus preserve seasonal signals of ISM rainfall (Breitenbach et al., 2010). Previous studies have indicated that variations in the $\delta^{18}\text{O}$ of speleothem calcite from Mawmluh Cave reflect changes in the amount-weighted $\delta^{18}\text{O}$ of precipitation ($\delta^{18}\text{O}_{\text{p}}$) values (Breitenbach et al., 2010, 2015; Berkelhammer et al., 2012; Myers et al., 2015). The ML.1 and ML.2 samples from Mawmluh Cave were collected in November 2015 at ~ 4–5 m above the cave floor

and ~ 700 m from the cave entrance. Diameters of ML.1 and ML.2 are ~ 170 and 165 mm, with lengths ~ 315 and ~ 311 mm, respectively. Both stalagmite samples were cut along their growth axes using a thin diamond blade. There are no visible changes in the texture or hiatuses in the above sample intervals that we used for this study (Fig. 3).

2.2 ^{230}Th dating

We obtained 18 and 5 ^{230}Th dates for samples ML.1 and ML.2, respectively. Subsamples for ^{230}Th dating (~ 30 mg) were drilled from ML.1 and ML.2 by using a 0.5 mm carbide dental drill. The ^{230}Th dating was performed at Xi’an Jiaotong University, China, using Thermo-Finnigan Neptune Plus multi-collector inductively coupled plasma mass spectrometers (MC-ICP-MSs). The method is described in Cheng et al. (2000, 2013). We used standard chemistry procedures (Edwards et al., 1987) to separate uranium and thorium. A triple-spike (^{229}Th – ^{233}U – ^{236}U) isotope dilution method was used to correct instrumental fractionation and to determine U/Th isotopic ratios and concentrations (Cheng et al., 2000,

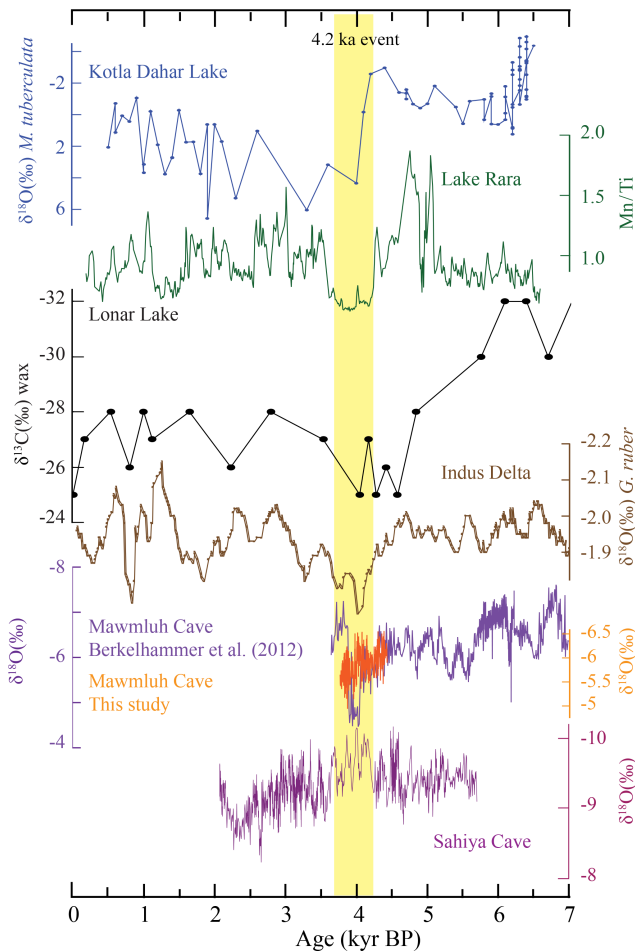


Figure 2. Proxy records from the Indian subcontinent. The select proxy records from the Indian monsoon domain from the top are Kotla Dhar (Dixit et al., 2014), Lake Rara (Nakamura et al., 2016), Lonar Lake (Sarkar et al., 2015), Indus Delta (Staubwasser et al., 2003), Mawmluh Cave (Berkelhammer et al., 2012; purple) and this study (orange), and Sahiya Cave (Kathayat et al., 2017). The yellow bar delineates the commonly accepted temporal duration of the 4.2 ka event (e.g., Weiss, 2016).

2013). U and Th isotopes were measured on a MasCom multiplier behind the retarding potential quadrupole in the peak-jumping mode using the standard procedures described in Cheng et al. (2000). Uncertainties in U/Th isotopic measurements were calculated offline at 2σ level, including corrections for blanks, multiplier dark noise, abundance sensitivity, and contents of the same nuclides in spike solution. The U decay constants are reported in Cheng et al. (2013). Corrected ^{230}Th ages assume the initial $^{230}\text{Th}/^{232}\text{Th}$ atomic ratio of $4.4 \pm 2.2 \times 10^{-6}$, the values for material at secular equilibrium with the bulk earth $^{232}\text{Th}/^{238}\text{U}$ value of 3.8. The corrections are small because the uranium concentrations of the samples are high (~ 6 ppm) and detrital ^{232}Th components are low (average < 170 ppt; Tables 1 and S1 in the Supplement).

2.3 Age models

The ML.1 age models and associated age uncertainties were constructed using the COPRA (Constructing Proxy Records from Age; Breitenbach et al., 2012), Bchron (Haslett and Parnell, 2008), and ISCAM (Fohlmeister, 2012) age modeling schemes (Fig. 4). All three modeling schemes yielded nearly identical results and the conclusions of this study are then not sensitive to the choice of different age models (Fig. 4). The ML.2 age model and associated uncertainties were constructed by only using the COPRA age modeling scheme (Breitenbach et al., 2012; Fig. 4).

2.4 Stable isotope analysis

The ML.1 and ML.2 $\delta^{18}\text{O}$ records are established by ~ 970 and ~ 238 stable isotope measurements, respectively (Figs. 5, 6 and Table S2). Subsamples for stable isotope measurements were obtained from ML.1 and ML.2 between depths of 125–250 and 182–255 mm (depth from the top), respectively. Accordingly, we report our data with zero depths set at 125 and 182 mm from the top of stalagmites ML.1 and ML.2, respectively (Fig. 3). We used New Wave Micromill, a digitally controlled triaxial micromill instrument, to obtain the subsamples. The sample growth rates were determined by sample age models, which in turn, were used to determine the subsampling increments (typically between 50 and 100 μm) for attaining similar temporal resolutions throughout the sample (typically ~ 1 year for the ML.1 $\delta^{18}\text{O}$ record). The $\delta^{18}\text{O}$ and $\delta^{13}\text{C}$ were measured using a Finnigan MAT-253 mass spectrometer coupled with an online carbonate preparation system (Kiel-IV) in the Isotope Laboratory, Xi'an Jiaotong University. Results are reported in per mil (‰) relative to the Vienna Pee Dee Belemnite (VPDB) standard. Duplicate measurements of standards NBS19 and TTB1 show a long-term reproducibility of ~ 0.1 ‰ (1σ) or better (Figs. 5, 6 and Table S2).

2.5 Replication and isotopic equilibrium

Excellent replication between the ML.1 and ML.2 $\delta^{18}\text{O}$ profiles (Fig. 5) suggests that the precipitation of speleothem calcite in Mawmluh Cave essentially occurred at or near isotopic equilibrium conditions and the speleothem $\delta^{18}\text{O}$ records primarily reflects the meteoric precipitation $\delta^{18}\text{O}$ variations (Dorale et al., 1998; Wang et al., 2001). A high degree of replication has been argued as a definitive test of isotopic equilibrium. This is because if the records replicate, the effect of additional kinetic and/or vadose-zone processes on the calcite $\delta^{18}\text{O}$ must have been either absent or exactly the same for spatially separated stalagmites. Principally, each speleothem–drip-water pair can have a distinctive combination of flow path, CO_2 content, residence time, solute concentrations, and prior calcite precipitation (PCP) history in the soil zone and epikarst above cave. Thus, the replication of different speleothem records suggests that such ad-

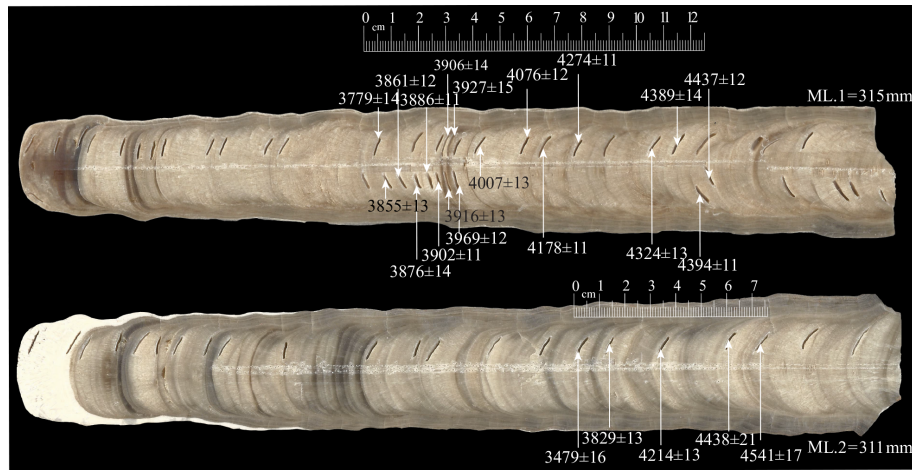


Figure 3. Samples photograph: the total length of ML.1 and ML.2 samples is 315 and 311 mm, respectively. The arrows indicate the dating subsampling location and the ^{230}Th dates with the 2σ analytical error (see also Tables 1 and S1). The centimeter scale indicates the location of isotopic measurements, enclosing the interval of interest within both the samples.

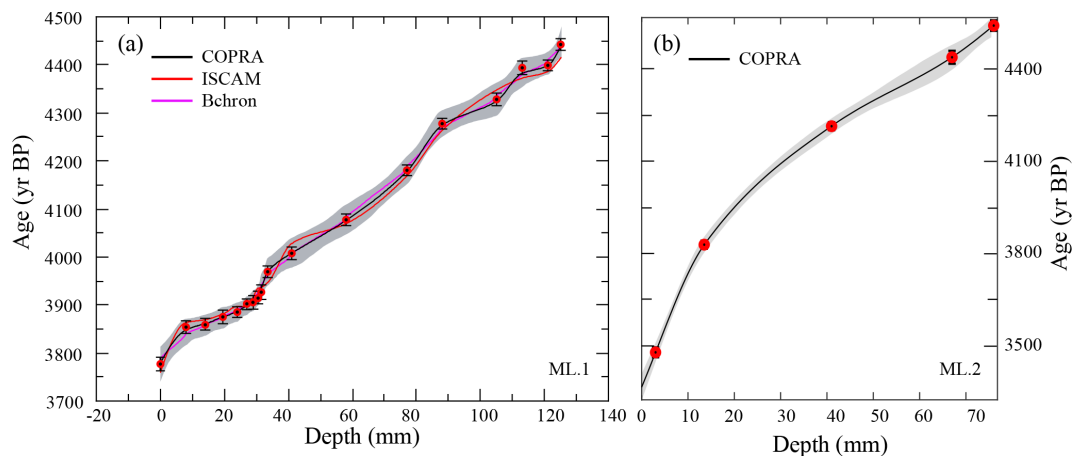


Figure 4. Age models of ML.1 and ML.2 records. We adopted COPRA and generated 2000 realizations of age models to account for the dating uncertainty (2.5 % and 97.5 % quantile) confidence limits. (a) ML.1 age models and modeled age uncertainties using three different age modeling algorithms: COPRA (black) (Breitenbach et al., 2012), Bchron (purple) (Haslett and Parnell, 2008), and ISCAM (red) (Fohlmeister, 2012). The gray band depicts the 95 % confidence interval using COPRA. Error bars on ^{230}Th dates represent a 2σ analytical error. (b) ML.2 age model and modeled age uncertainties using COPRA.

ditional processes are not crucial. We assessed the degree of replication between ML.1 and ML.2 $\delta^{18}\text{O}$ records by using the ISCAM (intra-site correlation age modeling) algorithm (Fohlmeister, 2012). The ISCAM finds the best correlation between proxy records within the combined age uncertainties of two records by using a Monte Carlo approach. Significant levels were calculated against a red-noise background from 1000 pairs of artificially simulated first-order autoregressive time series (AR1). The ML.1 and ML.2 $\delta^{18}\text{O}$ time series on ISCAM-derived age models display a statistically significant correlation ($r = 0.58$ at 95 % confidence level) over their contemporary growth period between ~ 4.4 and 3.8 ka.

3 Results

The average ^{230}Th dating uncertainties of the ML.1 and ML.2 records are ± 13 and ± 16 years, respectively (Fig. 3, Tables 1 and S1). Temporal resolutions of the ML.1 $\delta^{18}\text{O}$ record range from ~ 0.1 to ~ 3 years with an average resolution of ~ 1 year. All dates are in stratigraphic order within dating uncertainties. Of note, 9 ML.1 ^{230}Th dates were obtained between 27 and 88 mm depths (i.e., about one date every 7 mm), covering the interval from 4.2 to 3.9 ka, the typical time range of the 4.2 ka event. The ML.1 and ML.2 $\delta^{18}\text{O}$ values range between -6.6 and -4.8 ‰ with mean values of -5.80 and -5.43 ‰, respectively (Fig. 5). The average temporal resolution of the ML.2 record is ~ 5 years (Fig. 5). The

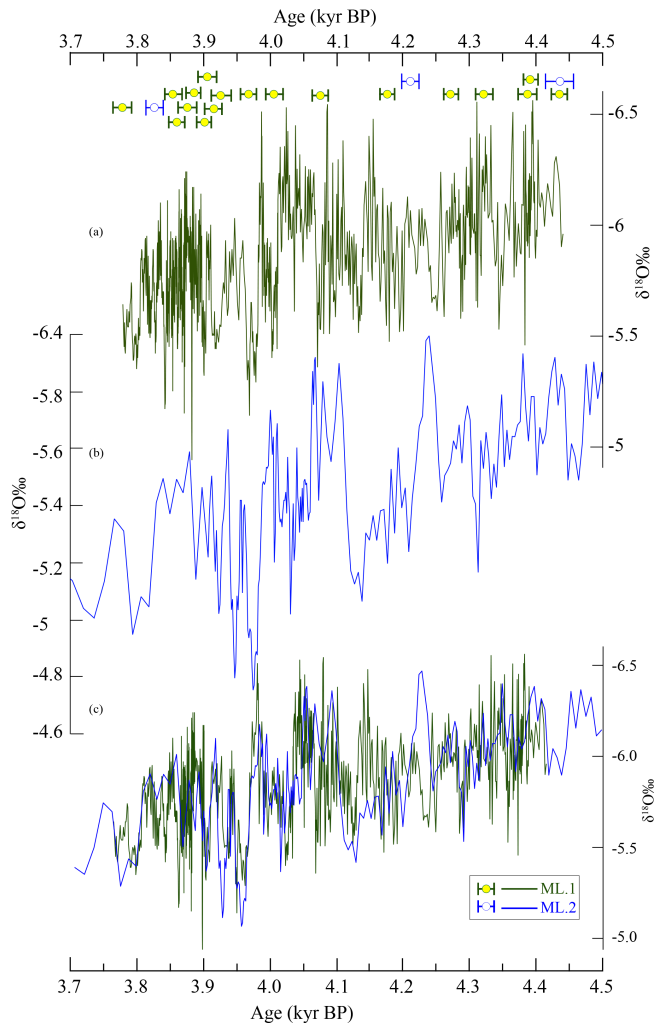


Figure 5. Comparison between ML.1 and ML.2 $\delta^{18}\text{O}$ profiles over the period of overlap. The ML.1 (a) and ML.2 (b) profiles are on their independent age models. The circles with horizontal error bars depict ^{230}Th dates and errors (2σ ; see also Tables 1, S1, and S2). (c) Comparison between the ML.1 and ML.2 $\delta^{18}\text{O}$ profiles based on the ISCAM algorithm (Fohlmeister, 2012).

$\delta^{13}\text{C}$ values in ML.1 and ML.2 range between -2.8‰ and 1.0‰ with mean values of -1.0‰ and -0.8‰ , respectively (Fig. 6).

4 Discussion and conclusions

4.1 Proxy interpretations

The temporal variability in ISM $\delta^{18}\text{O}_p$ and consequently speleothem $\delta^{18}\text{O}$ in the study area has been well studied previously and attributed mainly to changes in spatially integrated upstream rainfall at cave sites (e.g., Sinha et al., 2011a; Breitenbach et al., 2010, 2015; Berkelhammer et al., 2012; Kathayat et al., 2016; Cheng et al., 2016). A number of model simulations with isotope-enabled general cir-

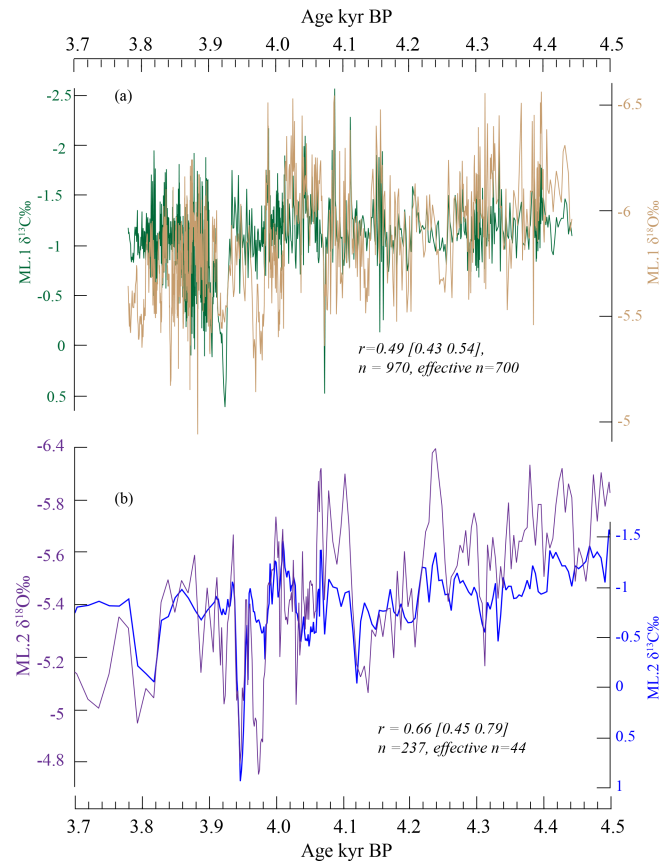


Figure 6. The $\delta^{18}\text{O}$ and $\delta^{13}\text{C}$ profiles of ML.1 and ML.2. (a) The ML.1 $\delta^{18}\text{O}$ (orange) and $\delta^{13}\text{C}$ (green). (b) The ML.2 $\delta^{18}\text{O}$ (purple) and $\delta^{13}\text{C}$ (blue) on their independent age models. The Pearson correlation (r) and its 95 % confidence interval together with actual and effective sample size (after considering autocorrelation in each profile) are shown in the figure.

ulation models (GCMs) also suggest a significant inverse relationship between upstream ISM rainfall amount and the $\delta^{18}\text{O}_p$ variations over the Indian subcontinent (e.g., Vuille et al., 2005; Pausata et al., 2011; Berkelhammer et al., 2012; Sinha et al., 2015; Midhun and Ramesh, 2016). Following these reasonings, we interpret the low and high $\delta^{18}\text{O}$ values in our records to reflect strong and weak ISM, respectively (e.g., Dayem et al., 2010; Sinha et al., 2011b, 2015; Cheng et al., 2012; Berkelhammer et al., 2012; Breitenbach et al., 2015; Myers et al., 2015; Kathayat et al., 2016, 2017). Climatic interpretations of the speleothem $\delta^{13}\text{C}$ signal, however, are more complex because the $\delta^{13}\text{C}$ variations can be driven by climatic changes and non-climate-related local processes (Baker et al., 1997; Genty et al., 2003; Fairchild and Treble, 2009; Fohlmeister et al., 2011; Deininger et al., 2012; Scholz et al., 2012). A moderate to strong covariance between the ML.1 and ML.2 $\delta^{13}\text{C}$ and $\delta^{18}\text{O}$ profile values ($r = 0.49$ and 0.66 , respectively) suggests that both proxies reflect a common response to changes in the local hydrology of the region;

however, we cannot rule out non-climate-related factors in producing this observed relationship. Consequently, the interpretative framework used in this study is mostly based on the speleothem $\delta^{18}\text{O}$ variability.

4.2 Comparisons between the KM-A and ML.1–ML.2 $\delta^{18}\text{O}$ records

The 4.2 ka event in the KM-A record (Berkelhammer et al., 2012) manifests as a two-step change marked by an initial increase in the $\delta^{18}\text{O}$ values ($\sim 0.6\text{‰}$) between ~ 4.31 and 4.30 ka, followed by another abrupt increase between ~ 4.07 and 4.05 ka. The period between 4.05 and 3.87 ka in the KM-A profile is characterized by the most enriched $\delta^{18}\text{O}$ values over the entire record ($\sim 1.5\text{‰}$ higher than the background values before the event; Fig. 7), delineating ~ 180 years of substantially weaker ISM. This multi-centennial period of enriched $\delta^{18}\text{O}$ values was terminated abruptly by a sharp return (< 20 years) to depleted $\delta^{18}\text{O}$ values, implying a resumption of stronger monsoon. The ML.1 and ML.2 $\delta^{18}\text{O}$ profiles during the contemporaneous period with the KM-A record, however, exhibit no step-like increase around ~ 4.3 ka but instead an abrupt increase in the $\delta^{18}\text{O}$ values at ~ 4.01 ka, which are superimposed over a gradually increasing trend over the entire length of the records. The timings and magnitude of this abrupt increase in the $\delta^{18}\text{O}$ values in both the ML.1 and ML.2 profiles are comparable to those observed in the KM-A profile (within the combined age uncertainties of both records; Fig. 7). A key difference between the KM-A, ML.1, and ML.2 $\delta^{18}\text{O}$ profiles, however, is the absence of a sharp decrease in the $\delta^{18}\text{O}$ values at ~ 3.87 ka in our records, which marks the termination of the 4.2 ka event in the KM-A record. One possible explanation for this apparent difference is the large uncertainties of the KM-A record. Another plausible source of the difference may stem from the dissolution of speleothem calcite in the KM-A sample between 0 and 29 mm depths (corresponding to ~ 3.65 and 5.08 ka; Fig. 7), which may have either altered the age of the top date of the KM-A (i.e., making it younger than its true age) or affected the $\delta^{18}\text{O}$ values of calcite during this period. However, without a comprehensive, petrographic examination of the KM-A sample, we are unable to assess the aforementioned reasons for such differences.

4.3 The ISM variability and possible climate forcing

The z -score-transformed ML.1 $\delta^{18}\text{O}$ profile (Fig. 8) illustrates the ISM variability between ~ 3.8 and 4.6 ka. The z score is calculated by using the equation of the form $z = (x - \mu)/\sigma$, where x represents the individual ML.1 $\delta^{18}\text{O}$ value, and μ and σ are the mean and the standard deviation of the entire ML.1 $\delta^{18}\text{O}$ record. The interval marking the onset of the 4.2 ka event in our record (~ 4.255 ka) is indicated by a transition from pluvial (inferred by the lower $\delta^{18}\text{O}$ values) to variable ISM (dry–wet) conditions, with the latter superim-

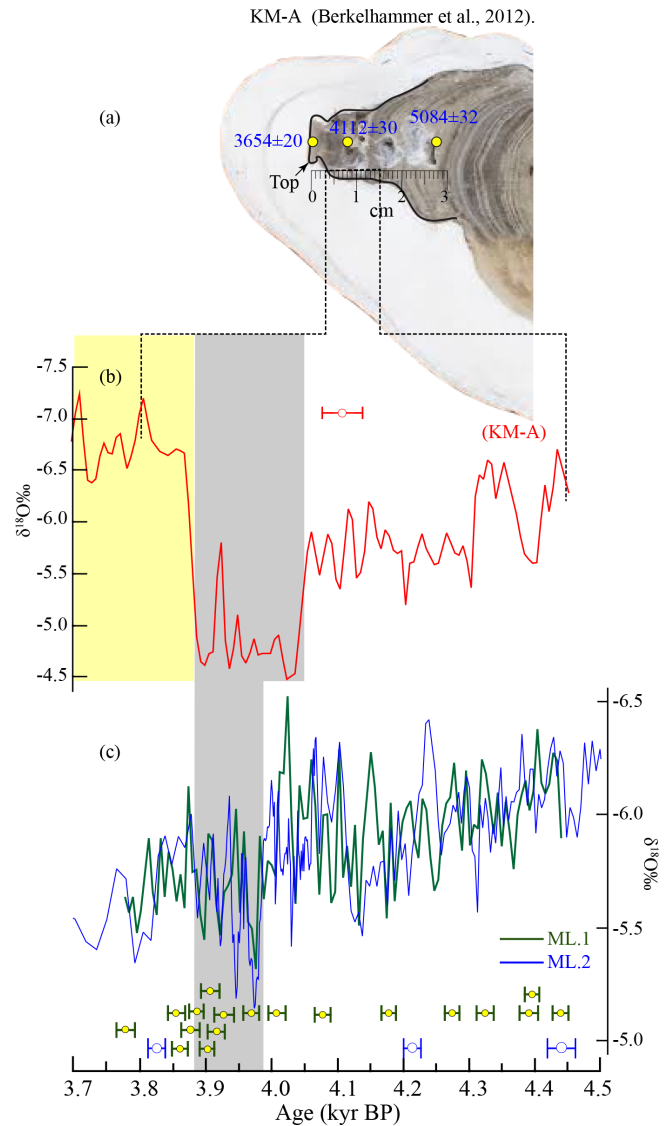


Figure 7. Comparison between the KM-A, ML.1, and ML.2 $\delta^{18}\text{O}$ profiles: (a) an image of KM-A stalagmite (Berkelhammer et al., 2012). The yellow dots indicate three ^{230}Th dates. The black curve marks the potential dissolution surface. The white aragonite layer above the dissolution surface was deposited after the 1950s with the advent of limestone mining above the Mawmluh Cave (Breitenbach et al., 2010). (b) The dotted lines delineate the portion of the KM-A $\delta^{18}\text{O}$ record (red; ~ 4.4 ka to 3.654 ka) (Berkelhammer et al., 2012) discussed in the text. (c) The ML.2 $\delta^{18}\text{O}$ profile (blue) (this study) is overlaid by a 6-year interpolated ML.1 $\delta^{18}\text{O}$ profile (green) (this study; see also Table S2). The horizontal error bars (red, green, and blue) on the ^{230}Th dates represent a 2σ analytical error. The vertical gray bar indicates the inferred duration of weakest (driest phase) ISM as indicated by the KM-A and ML $\delta^{18}\text{O}$ records. The yellow bar indicates the interval of anomalously depleted $\delta^{18}\text{O}$ values in the KM-A record.

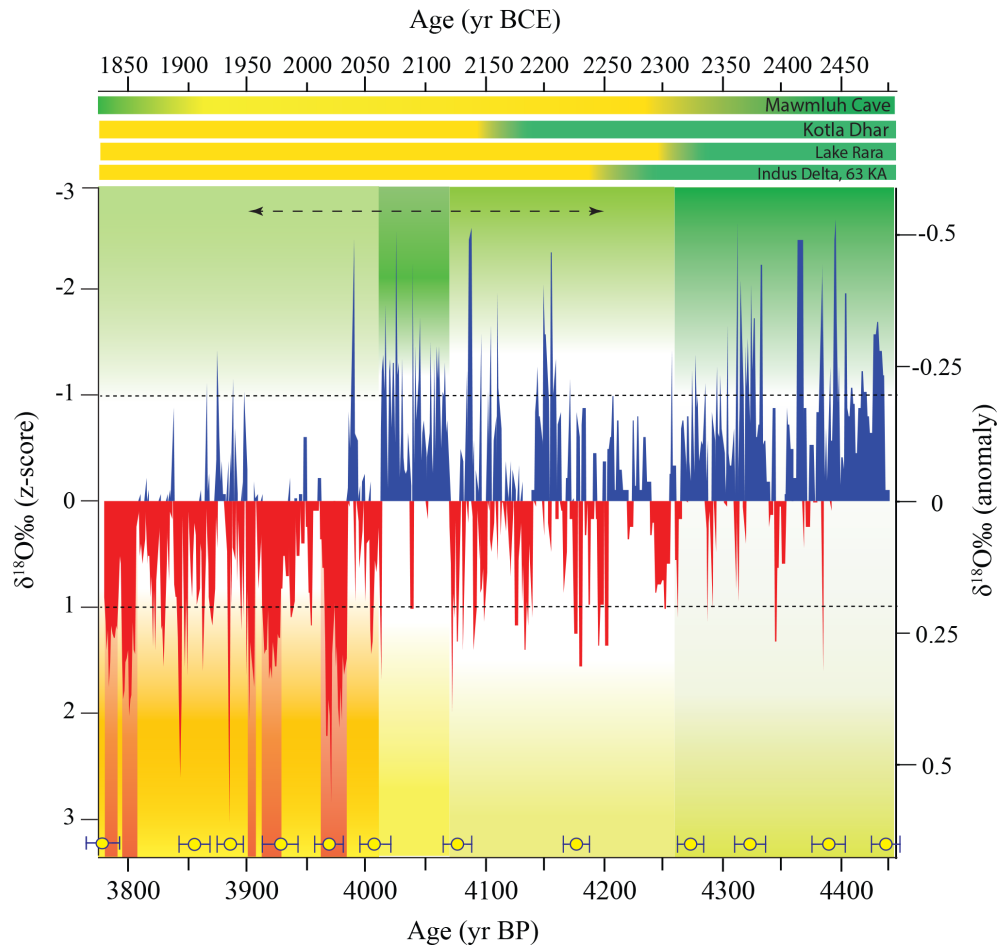


Figure 8. The inferred pattern of ISM variability during the 4.2 ka event: the ML.1 $\delta^{18}\text{O}$ record is shown here as z score (left y axis) and anomalies (right y axis). The horizontal dashed lines indicate 1 standard deviation and the vertical color-saturated shaded bars denote periods of inferred drier (yellow) pluvial (green) and variable conditions. The vertical red bars delineate the periods of multi-decadal droughts (z score > 1). The horizontal dashed double arrows mark the commonly accepted duration of the 4.2 ka event (see text) and the horizontal shaded bars indicate broad hydroclimate patterns inferred from other regional proxy records as mentioned in the text (see also Figs. 1 and 2). The circles with 2σ error bars show a subset of ^{230}Th dates (see Tables 1 and S1 for a complete listing of ^{230}Th dates).

posed by a few short-term ($< \text{decade}$) droughts (Fig. 8). Subsequently, the period between 4.07 and ~ 4.01 ka is marked by persistently lower $\delta^{18}\text{O}$ values, implying stronger ISM (Fig. 8). The latter was terminated by a rapid increase in the $\delta^{18}\text{O}$ values ($\sim 1.0\text{‰}$, Fig. 5), suggesting an abrupt weakening of the ISM at ~ 4.01 ka that occurred within a period of ~ 10 years. Notably, as discussed above, the ML.1 and ML.2 $\delta^{18}\text{O}$ profiles show gradual increasing trends over the entire length of the record, which was punctuated by two multi-decadal weak monsoon events centered at ~ 3.970 (~ 20 years) and ~ 3.915 ka (~ 25 years), respectively (Fig. 8). These aspects of our ISM reconstruction differ from previous proxy records from the ISM domain, which typically portray the 4.2 ka event as a multi-century drought (e.g., Berkelhammer et al., 2012; Dixit et al., 2014). Our new data, however, demonstrate that prominent decadal to multi-decadal variability, together with the intermittent occurrence of multi-

decadal periods of low rainfall, was the dominant mode of ISM variability during the period coeval with the 4.2 ka event (Figs. 5 and 8). These observations are consistent with previous reconstructions of ISM variability from high-resolution proxy records from the Indian subcontinent over the last 2 millennia (e.g., Sinha et al., 2011a, 2015; Kathayat et al., 2017) as well as during the instrumental period (e.g., Krishnamurthy and Shukla, 2000; Goswami et al., 2006). Periodic perturbations in coupled modes of ocean–atmosphere variability, such as the El Niño–Southern Oscillation (ENSO), and/or dynamical processes intrinsic to the monsoon system, such as quasi-periodic episodes of intense (“active”) and reduced (“break”) monsoon rainfall, are key processes that are known to produce multi-decadal periods of droughts over large parts of Asia. For instance, Sinha et al. (2011b) suggest that ISM circulation can “lock” into decadal to multi-decadal periods of a “break-dominated” mode of ISM cir-

ulation that promotes enhanced convection over the eastern equatorial Indian Ocean, which in turn suppresses convection and rainfall over the continental monsoon regions. Additionally, the source of multi-decadal droughts may stem from the switch-on of the modern ENSO regime around the 4.2 ka event, which would presumably also weaken the ISM (e.g., Donders et al., 2008; Conroy et al., 2008).

In conclusion, our new record from the Mawmluh Cave in Meghalaya, India, provides a high-resolution history of ISM during a period contemporaneous with the 4.2 ka event. While our record shares broad similarities with a previous lower-resolution (~ 6 years) reconstruction of ISM from the same cave (Berkelhammer et al., 2012), key differences between the two records are also evident, which are likely due to the more refined age controls (approximately nine ^{230}Th dates spanning the 4.2 ka event interval and the higher (annual) temporal resolution of our record). Our reconstruction suggests that the ISM exhibited prominent decadal to multi-centennial variability, including sporadic but prominent multi-decadal periods of reduced ISM rainfall (droughts), during the period spanning the 4.2 ka event. These aspects of our reconstruction are qualitatively similar to ISM variability during the late and middle Holocene as inferred from the previous speleothem-based reconstructions of ISM from the Indian subcontinent (e.g., Kathayat et al., 2017).

Data availability. All data needed to evaluate the conclusions in the paper are presented in the paper. Additional data related to this paper may be requested from the authors. The data will be archived at the NOAA National Climate Data Center (<https://www.ncdc.noaa.gov/data-access/paleoclimatology-data>, last access: 26 November 2018). Correspondence and requests for materials should be addressed to Gayatri Kathayat (kathayatg@xjtu.edu.cn) and Hai Cheng (cheng021@xjtu.edu.cn).

Author contributions. GK and HC designed the research and experiments. GK wrote the first draft of the paper. HC, AS, and MB revised the paper. GK, HC, and XL did the fieldwork and collected the samples. GK, HC, HZ, and RLE conducted the ^{230}Th dating. GK, PD, and HL conducted the oxygen isotope measurements. All authors discussed the results and provided inputs on the paper.

Competing interests. The authors declare that they have no conflict of interest.

Special issue statement. This article is part of the special issue “The 4.2 ka BP climatic event”. It is a result of “The 4.2 ka BP Event: An International Workshop”, Pisa, Italy, 10–12 January 2018.

Acknowledgements. We thank Giovanni Zanchetta and the two anonymous reviewers for their comments that helped improve the original paper. We thank Digambar Singh Chauhan, Chetan Singh Chauhan, Aditya Singh Kathayat, Geetanjali Kathayat, Neha Pant, Sanjay Melkani, Clive Dunnai, Ardy Dunnai, and Ceejey Dunnai for their assistance during the fieldwork. This work is supported by grants from the Natural Science Foundation of China to Gayatri Kathayat (NSFC 41703007), Hai Cheng (NSFC 41731174 and 4157020432), R. Lawrence Edwards and Hai Cheng (NSF 1702816), and Haiwei Zhang (NSFC 41502166).

Edited by: Giovanni Zanchetta

Reviewed by: two anonymous referees

References

- Arz, H. W., Lamy, F., and Pätzold, J.: A pronounced dry event recorded around 4.2 ka in brine sediments from the northern Red Sea, *Quaternary Res.*, 66, 432–441, 2006.
- Baker, A., Ito, E., Smart, P. L., and McEwan, R. F.: Elevated and variable values of ^{13}C in speleothems in a British cave system, *Chem. Geol.*, 136, 263–270, 1997.
- Berkelhammer, M., Sinha, A., Stott, L., Cheng, H., Pausata, F., and Yoshimura, K.: An abrupt shift in the Indian monsoon 4000 years ago, *Geophys. Monogr. Ser.*, 198, 75–88, 2012.
- Breitenbach, S. F., Adkins, J. F., Meyer, H., Marwan, N., Kumar, K. K., and Haug, G. H.: Strong influence of water vapor source dynamics on stable isotopes in precipitation observed in Southern Meghalaya, NE India, *Earth Planet. Sc. Lett.*, 292, 212–220, 2010.
- Breitenbach, S. F. M., Rehfeld, K., Goswami, B., Baldini, J. U. L., Ridley, H. E., Kennett, D. J., Prufer, K. M., Aquino, V. V., Asmerom, Y., Polyak, V. J., Cheng, H., Kurths, J., and Marwan, N.: COConstructing Proxy Records from Age models (CO-PRA), *Clim. Past*, 8, 1765–1779, <https://doi.org/10.5194/cp-8-1765-2012>, 2012.
- Breitenbach, S. F. M., Lechleitner, F. A., Meyer, H., Diengdoh, G., Matthey, D., and Marwan, N.: Cave ventilation and rainfall signals in dripwater in a monsoonal setting – a monitoring study from NE India, *Chem. Geol.*, 402, 111–124, 2015.
- Chang, K. C.: China on the eve of the Historical Period, in: *The Cambridge History of Ancient China – From the Origins of Civilization to 221 BC*, edited by: Loewe, M. and Shaughnessy, E. L., Cambridge University Press, New York, 37–73, 1999.
- Cheng, H., Edwards, R., Hoff, J., Gallup, C., Richards, D., and Asmerom, Y.: The half-lives of uranium-234 and thorium-230, *Chem. Geol.*, 169, 17–33, 2000.
- Cheng, H., Zhang, P., Spötl, C., Edwards, R., Cai, Y., Zhang, D., Sang, W., Tan, M., and An, Z.: The climatic cyclicity in semiarid central Asia over the past 500,000 years, *Geophys. Res. Lett.*, 39, L01705, <https://doi.org/10.1029/2011GL050202>, 2012.
- Cheng, H., Edwards, R. L., Shen, C.-C., Polyak, V. J., Asmerom, Y., Woodhead, J., Hellstrom, J., Wang, Y., Kong, X., and Spötl, C.: Improvements in ^{230}Th dating, ^{230}Th and ^{234}U half-life values, and U–Th isotopic measurements by multi-collector inductively coupled plasma mass spectrometry, *Earth Planet. Sc. Lett.*, 371, 82–91, 2013.

- Cheng, H., Sinha, A., Verheyden, S., Nader, F. H., Li, X. L., Zhang, P. Z., Yin, J. J., Yi, L., Peng, Y. B., Rao, Z. G., Ning, Y. F., and Edwards, R. L.: The climate variability in northern Levant over the past 20,000 years, *Geophys. Res. Lett.*, 42, 8641–8650, 2015.
- Cheng, H., Edwards, R. L., Sinha, A., Spötl, C., Yi, L., Chen, S., Kelly, M., Kathayat, G., Wang, X., and Li, X.: The Asian monsoon over the past 640,000 years and ice age terminations, *Nature*, 534, 640–646, 2016.
- Conroy, J. L., Overpeck, J. T., Cole, J. E., Shanahan, T. M., and Steinitz-Kannan, M.: Holocene changes in eastern tropical Pacific climate inferred from a Galápagos lake sediment record, *Quaternary Sci. Rev.*, 27, 1166–1180, 2008.
- Cullen, H. M., Hemming, S., Hemming, G., Brown, F., Guilderson, T., and Sirocko, F.: Climate change and the collapse of the Akkadian empire: Evidence from the deep sea, *Geology*, 28, 379–382, 2000.
- Dayem, K. E., Molnar, P., Battisti, D. S., and Roe, G. H.: Lessons learned from oxygen isotopes in modern precipitation applied to interpretation of speleothem records of paleoclimate from eastern Asia, *Earth Planet. Sc. Lett.*, 295, 219–230, 2010.
- Deininger, M., Fohlmeister, J., Scholz, D., and Mangini, A.: Isotope disequilibrium effects: The influence of evaporation and ventilation effects on the carbon and oxygen isotope composition of speleothems – A model approach, *Geochim. Cosmochim. Ac.*, 96, 57–79, 2012.
- Dixit, Y., Hodell, D. A., and Petrie, C. A.: Abrupt weakening of the summer monsoon in northwest India ~ 4100 yr ago, *Geology*, 42, 339–342, 2014.
- Dixit, Y., Hodell, D. A., Giesche, A., Tandon, S. K., Gázquez, F., Saini, H. S., Skinner, L. C., Mujtaba, S. A., Pawar, V., and Singh, R. N.: Intensified summer monsoon and the urbanization of Indus Civilization in northwest India, *Sci. Rep.-UK*, 8, 4225, <https://doi.org/10.1038/s41598-018-22504-5>, 2018.
- Donders, T. H., Wagner-Cremer, F., and Visscher, H.: Integration of proxy data and model scenarios for the mid-Holocene onset of modern ENSO variability, *Quaternary Sci. Rev.*, 27, 571–579, 2008.
- Dorale, J. A., Edwards, R. L., Ito, E., and González, L. A.: Climate and Vegetation History of the Midcontinent from 75 to 25 ka: A Speleothem Record from Crevice Cave, Missouri, USA, *Science*, 282, 1871–1874, 1998.
- Drysdale, R., Zanchetta, G., Hellstrom, J., Maas, R., Fallick, A., Pickett, M., Cartwright, I., and Piccini, L.: Late Holocene drought responsible for the collapse of Old World civilizations is recorded in an Italian cave flowstone, *Geology*, 34, 101–104, 2006.
- Edwards, R. L., Chen, J., and Wasserburg, G.: ^{238}U ^{234}U ^{230}Th ^{232}Th systematics and the precise measurement of time over the past 500,000 years, *Earth Planet. Sc. Lett.*, 81, 175–192, 1987.
- Enzel, Y., Ely, L. L., Mishra, S., Ramesh, R., Amit, R., Lazar, B., Rajaguru, S. N., Baker, V. R., and Sandler, A.: High-resolution Holocene environmental changes in the Thar Desert, northwestern India, *Science*, 284, 125–128, 1999.
- Fairchild, I. J. and Treble, P. C.: Trace elements in speleothems as recorders of environmental change, *Quaternary Sci. Rev.*, 28, 449–468, 2009.
- Fohlmeister, J.: A statistical approach to construct composite climate records of dated archives, *Quat. Geochronol.*, 14, 48–56, 2012.
- Fohlmeister, J., Scholz, D., Kromer, B., and Mangini, A.: Modelling carbon isotopes of carbonates in cave drip water, *Geochim. Cosmochim. Ac.*, 75, 5219–5228, 2011.
- Genty, D., Blamart, D., Ouahdi, R., Gilmour, M., Baker, J., Jouzel, J., and Van-Exter, S.: Precise dating of Dansgaard-Oeschger climate oscillations in western Europe from stalagmite data, *Nature*, 421, 833–837, 2003.
- Giosan, L., Clift, P. D., Macklin, M. G., Fuller, D. Q., Constantinescu, S., Durcan, J. A., Stevens, T., Duller, G. A., Tabrez, A. R., and Gangal, K.: Fluvial landscapes of the Harappan civilization, *P. Natl. Acad. Sci. USA*, 109, E1688–E1694, 2012.
- Goswami, B. N., Wu, G., and Yasunari, T.: The annual cycle, intraseasonal oscillations, and roadblock to seasonal predictability of the Asian summer monsoon, *J. Climate*, 19, 5078–5098, 2006.
- Haslett, J. and Parnell, A.: A simple monotone process with application to radiocarbon-dated depth chronologies, *J. R. Stat. Soc. C-Appl.*, 57, 399–418, 2008.
- Kathayat, G., Cheng, H., Sinha, A., Spötl, C., Edwards, R. L., Zhang, H., Li, X., Yi, L., Ning, Y., Cai, Y., Lui, W. L., and Breitenbach, S. F. M.: Indian monsoon variability on millennial-orbital timescales, *Sci. Rep.-UK*, 6, 24374, <https://doi.org/10.1038/srep24374>, 2016.
- Kathayat, G., Cheng, H., Sinha, A., Yi, L., Li, X., Zhang, H., Li, H., Ning, Y., and Edwards, R. L.: The Indian monsoon variability and civilization changes in the Indian subcontinent, *Science Advances*, 3, e1701296, <https://doi.org/10.1126/sciadv.1701296>, 2017.
- Krishnamurthy, V. and Shukla, J.: Intraseasonal and interannual variability of rainfall over India, *J. Climate*, 13, 4366–4377, 2000.
- Liu, F. and Feng, Z.: A dramatic climatic transition at ~ 4000 cal. yr BP and its cultural responses in Chinese cultural domains, *Holocene*, 22, 1181–1197, 2012.
- Madella, M. and Fuller, D. Q.: Palaeoecology and the Harappan Civilisation of South Asia: a reconsideration, *Quaternary Sci. Rev.*, 25, 1283–1301, 2006.
- Marshall, M. H., Lamb, H. F., Huws, D., Davies, S. J., Bates, R., Bloemendal, J., Boyle, J., Leng, M. J., Umer, M., and Bryant, C.: Late Pleistocene and Holocene drought events at Lake Tana, the source of the Blue Nile, *Global Planet. Change*, 78, 147–161, 2011.
- Menounos, B., Clague, J. J., Osborn, G., Luckman, B. H., Lake-man, T. R., and Minkus, R.: Western Canadian glaciers advance in concert with climate change circa 4.2 ka, *Geophys. Res. Lett.*, 35, <https://doi.org/10.1029/2008GL033172>, 2008.
- Midhun, M. and Ramesh, R.: Validation of $\delta^{18}\text{O}$ as a proxy for past monsoon rain by multi-GCM simulations, *Clim. Dynam.*, 46, 1371–1385, 2016.
- Murata, F., Hayashi, T., Matsumoto, J., and Asada, H.: Rainfall on the Meghalaya plateau in northeastern India – one of the rainiest places in the world, *Nat. Hazards*, 42, 391–399, 2007.
- Myers, C. G., Oster, J. L., Sharp, W. D., Bennartz, R., Kelley, N. P., Covey, A. K., and Breitenbach, S. F.: Northeast Indian stalagmite records Pacific decadal climate change: Implications for moisture transport and drought in India, *Geophys. Res. Lett.*, 42, 4124–4132, 2015.
- Nakamura, A., Yokoyama, Y., Maemoku, H., Yagi, H., Okamura, M., Matsuoka, H., Miyake, N., Osada, T., Adhikari, D. P., and Dangol, V.: Weak monsoon event at 4.2 ka recorded in sedi-

- ment from Lake Rara, Himalayas, *Quaternary Int.*, 397, 349–359, 2016.
- Pausata, F. S., Battisti, D. S., Nisancioglu, K. H., and Bitz, C. M.: Chinese stalagmite $\delta^{18}\text{O}$ controlled by changes in the Indian monsoon during a simulated Heinrich event, *Nat. Geosci.*, 4, 474–480, 2011.
- Prasad, S. and Enzel, Y.: Holocene paleoclimates of India, *Quaternary Res.*, 66, 442–453, 2006.
- Railsback, L. B., Liang, F., Brook, G., Voarintsoa, N. R. G., Sletten, H. R., Marais, E., Hardt, B., Cheng, H., and Edwards, R. L.: The timing, two-pulsed nature, and variable climatic expression of the 4.2 ka event: A review and new high-resolution stalagmite data from Namibia, *Quaternary Sci. Rev.*, 186, 78–90, 2018.
- Sarkar, S., Prasad, S., Wilkes, H., Riedel, N., Stebich, M., Basavaiah, N., and Sachse, D.: Monsoon source shifts during the drying mid-Holocene: Biomarker isotope based evidence from the core “monsoon zone” (CMZ) of India. *Quaternary Sci. Rev.*, 123, 144–157, 2015.
- Sabin, T., Krishnan, R., Ghattas, J., Denvil, S., Dufresne, J.-L., Hourdin, F., and Pascal, T.: High resolution simulation of the South Asian monsoon using a variable resolution global climate model, *Clim. Dynam.*, 41, 173–194, 2013.
- Scholz, D., Frisia, S., Borsato, A., Spötl, C., Fohlmeister, J., Mudelsee, M., Miorandi, R., and Mangini, A.: Holocene climate variability in north-eastern Italy: potential influence of the NAO and solar activity recorded by speleothem data, *Clim. Past*, 8, 1367–1383, <https://doi.org/10.5194/cp-8-1367-2012>, 2012.
- Sengupta, S. and Sarkar, A.: Stable isotope evidence of dual (Arabian Sea and Bay of Bengal) vapour sources in monsoonal precipitation over north India, *Earth Planet. Sc. Lett.*, 250, 511–521, 2006.
- Sinha, A., Berkelhammer, M., Stott, L., Mudelsee, M., Cheng, H., and Biswas, J.: The leading mode of Indian Summer Monsoon precipitation variability during the last millennium, *Geophys. Res. Lett.*, 38, L15703, <https://doi.org/10.1029/2011GL047713>, 2011a.
- Sinha, A., Stott, L., Berkelhammer, M., Cheng, H., Edwards, R. L., Buckelew, B., Aldenderfer, M., and Mudelsee, M.: A global context for megadroughts in monsoon Asia during the past millennium, *Quaternary Sci. Rev.*, 30, 47–62, 2011b.
- Sinha, A., Kathayat, G., Cheng, H., Breitenbach, S. F., Berkelhammer, M., Mudelsee, M., Biswas, J., and Edwards, R.: Trends and oscillations in the Indian summer monsoon rainfall over the last two millennia, *Nat. Commun.*, 6, 6309, <https://doi.org/10.1038/ncomms7309>, 2015.
- Stanley, J.-D., Krom, M. D., Cliff, R. A., and Woodward, J. C.: Nile flow failure at the end of the Old Kingdom, Egypt: strontium isotopic and petrologic evidence, *Geoarchaeology Int. J.*, 18, 395–402, 2003.
- Staubwasser, M. and Weiss, H.: Holocene Climate and Cultural Evolution in Late Prehistoric-Early Historic West Asia, *Quaternary Res.*, 66, 372–387, 2006.
- Staubwasser, M., Sirocko, F., Grootes, P., and Segl, M.: Climate change at the 4.2 ka BP termination of the Indus valley civilization and Holocene south Asian monsoon variability, *Geophys. Res. Lett.*, 30, 1425, <https://doi.org/10.1029/2002GL016822>, 2003.
- Vuille, M., Werner, M., Bradley, R. S., and Keimig, F.: Stable isotopes in precipitation in the Asian monsoon region, *J. Geophys. Res.-Atmos.*, 110, D23108, <https://doi.org/10.1029/2005JD006022>, 2005.
- Walker, M., Head, M. J., Berkelhammer, M., Björck, S., Cheng, H., Cwynar, L., Fisher, D., Gkinis, V., Long, A., Lowe, J., Newnham, R., Olander, R. S., and Weiss, H.: Formal ratification of the subdivision of the Holocene Series/Epoch (Quaternary System/Period): two new Global Boundary Stratotype Sections and Points (GSSPs) and three new stages/subseries, *IUGS*, 1–11, 2018.
- Wang, Y. J., Cheng, H., Edwards, R. L., An, Z. S., Wu, J. Y., Shen, C. C., and Dorale, A. J.: A high-Resolution Absolute-Dated Late Pleistocene Monsoon Record from Hulu Cave, China, *Science*, 294, 2345–2348, 2001.
- Weiss, H.: Global megadrought, societal collapse and resilience at 4.2–3.9 ka BP across the mediterranean and west asia, *PAGES*, 24, 62–63, 2016.
- Weiss, H., Courty, M.-A., Wetterstrom, W., Guichard, F., Senior, L., Meadow, R., and Curnow, A.: The genesis and collapse of third millennium north Mesopotamian civilization, *Science*, 261, 995–1004, 1993.